Role of S65, Q67, I68, and Y69 Residues in Homotetrameric R67 Dihydrofolate Reductase†

Michael Brad Strader, R. Derike Smiley, Lori G. Stinnett, Nathan C. VerBerkmoes, and Elizabeth E. Howell*

Department of Biochemistry and Cellular and Molecular Biology, University of Tennessee, Knoxville, Tennessee 37996-0840

Received May 22, 2001; Revised Manuscript Received July 31, 2001

ABSTRACT: R67 dihydrofolate reductase (DHFR) shares no sequence or structural homology with chromosomal DHFRs. This enzyme arose recently in response to the clinical use of the antibacterial drug trimethoprim. R67 DHFR is a homotetramer possessing a single active site pore. A high-resolution crystal structure shows the homotetramer possesses exact 222 symmetry [Narayana, N., et al. (1995) *Nat. Struct. Biol. 2*, 1018−1025]. This symmetry dictates four symmetry-related binding sites must exist for each substrate as well as each cofactor. Isothermal titration calorimetry studies, however, indicate only two molecules bind: either two dihydrofolate molecules, two NADPH molecules, or one substrate and one cofactor [Bradrick, T. D., et al. (1996) *Biochemistry 35*, 11414−11424]. The latter is the productive ternary complex. To evaluate the role of S65, Q67, I68, and Y69 residues, located near the center of the active site pore, site-directed mutagenesis was performed. One mutation in the gene creates four mutations per active site pore which typically result in large cumulative effects. Steady state kinetic data indicate the mutants have altered K_m values for both cofactor and substrate. For example, the Y69F R67 DHFR displays an 8-fold increase in the K_m for dihydrofolate and a 20-fold increase in the K_m for NADPH. Residues involved in ligand binding in R67 DHFR display very little, if any, specificity, consistent with their possessing dual roles in binding. These results support a model where R67 DHFR utilizes an unusual "hot spot" binding surface capable of binding both ligands and indicate this enzyme has adopted a novel yet simple approach to catalysis.

Dihydrofolate reductase (DHFR)[1] reduces dihydrofolate (DHF) to tetrahydrofolate using NADPH as a cofactor. It catalyzes an important step in folate metabolism since tetrahydrofolate is involved in the synthesis of thymidylate, purine nucleosides, methionine, and other metabolic intermediates. DHFR is a target for clinically important drugs such as methotrexate and trimethoprim since efficient inhibition of its activity culminates in blockage of DNA synthesis and cell death.

Trimethoprim (TMP), an active site-directed inhibitor of chromosomally encoded bacterial DHFRs, is used to treat bacterial infections. Resistance to trimethoprim (TMP) has been observed and correlated with the production of novel DHFRs encoded by R-plasmids. Type II R-plasmid-encoded R67 DHFR is genetically and structurally unrelated to chromosomal DHFRs; thus, a comparison of its properties with those of chromosomal DHFR can elucidate differences in their catalytic strategies.

R67 DHFR was initially crystallized as a dimer (*1*). More recently, a crystal structure of the active homotetramer was reported, both as an apoenzyme and as a binary complex with folate (*2*). Each monomer of R67 DHFR possesses a five-stranded β-barrel fold that has subsequently been identified as occurring in SH3 domains.[2] The R67 DHFR tetramer displays a toroidal shape with a pore that traverses the length of the protein. This pore has been identified as the active site by difference Fourier maps describing bound folate. While a shared active site between protomers is not surprising, only one active site per oligomer is quite unusual. Other examples of one binding site per oligomer include the AIDS protease (*3*), 3,5,3′,5′-tetraiodo-L-thyronine (T_4) binding to transthyretin (*4*), and bisphosphoglycerate binding to the central pore in hemoglobin (*5*).

A 222 symmetry operator occurs at the center of the active site pore; this dictates that for each binding site, there must be three symmetry-related sites generated by 180° rotations along the *x*, *y*, and *z* axes. Once a ligand binds, however, then R67 DHFR no longer possesses 222 symmetry. As long as the asymmetry does not affect lattice interactions, overall 222 symmetry in the crystal can still be preserved by disordering where the asymmetric molecules randomly occupy the four symmetry-related binding sites. This situation describes the R67 DHFR·folate complex (*2*). Difference

† This research was supported by NSF Grant MCB-9808302 (to E.E.H.).

* To whom correspondence should be addressed. Phone: (865) 974-4507. Fax: (865) 974-6306. E-mail: lzh@utk.edu.

[1] Abbreviations: DHFR, dihydrofolate reductase; wt, wild type; TMP, trimethoprim; DHF, dihydrofolate; $NADP^+$ and NADPH, oxidized and reduced nicotinamide adenine dinucleotide phosphate, respectively; NMN, nicotinamide mononucleotide; MTA buffer, 100 mM Tris, 50 mM MES, and 50 mM acetic acid polybuffer; ITC, isothermal titration calorimetry; CD, circular dichroism. Mutant enzymes containing amino acid substitutions are described by the wild-type residue and numbered position in the sequence, followed by the amino acid substitution. For example, Q67C R67 DHFR describes the Gln67 → Cys mutant.

[2] The amino acids in the first monomer are labeled 1−78, those in the second monomer 101−178, those in the third monomer 201−278, and those in the fourth monomer 301−378. For brevity, when a single residue is mentioned, all four symmetry-related residues are implied.

10.1021/bi0110544 CCC: $20.00
Published on Web 08/30/2001

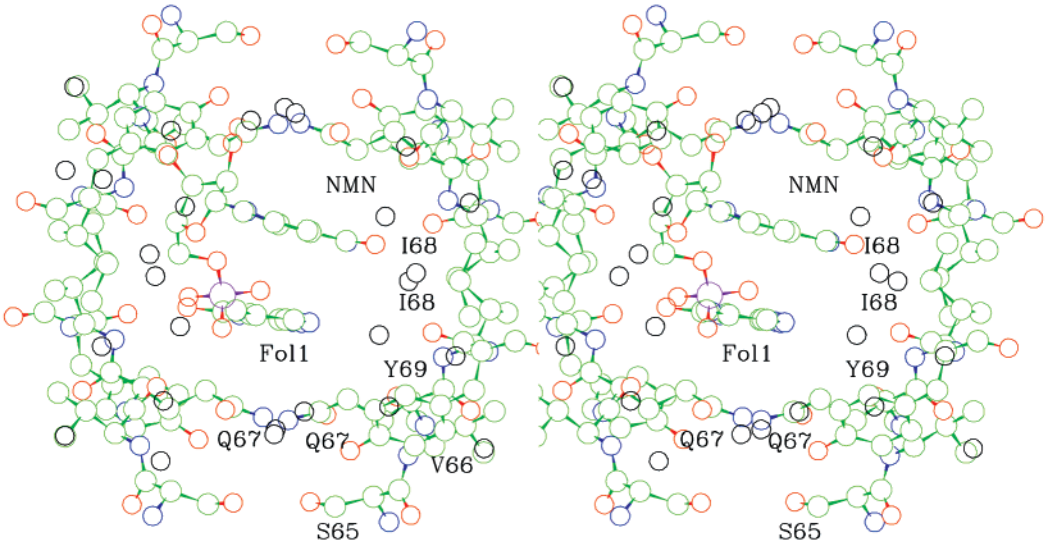

FIGURE 1: Stereodrawing of the active site pore in R67 DHFR. The Fol1 molecule was obtained from Protein Data Bank entry 1VIF. The NMN molecule was docked into the R67 DHFR·Fol1 complex using DOCK (E. E. Howell et al., manuscript submitted for publication). Residues 65−69 are labeled for one monomer (bottom right). The same residues repeat three additional times due to the 222 symmetry. A second Q67 residue is labeled at the bottom left; a second I68 residue is labeled at the middle right. Green denotes carbon atoms, blue nitrogen atoms, red oxygen atoms, magenta phosphorus atoms, and black water molecules.

maps for bound folate show low density in the pore and describe overlapping density from two folate molecules bound in two asymmetric sites (Fol1 and Fol2), each at 1/4 occupancy.

Our binding studies using isothermal titration calorimetry (ITC) show only two molecules bind concurrently, most likely due to steric constraints. The combinations of bound molecules include two substrates (dihydrofolate or folate), two cofactors (NADPH), or one substrate and one cofactor (*6*). The latter is the productive, ternary complex. Cofactor inhibition is not typically observed (within the range of assay concentrations that were used) as negative cooperativity occurs between two bound NADPH molecules (macroscopic K_d values of 2.5 and 95 μM). Substrate inhibition is also not typically observed as positive cooperativity between two bound dihydrofolate molecules occurs (macroscopic K_d values of 125 and 8.8 μM). This model indicates each half-pore can accommodate either DHF and folate or NADPH, presumably with different orientations.

Serine 65 (S65), glutamine 67 (Q67), isoleucine 68 (I68), and tyrosine 69 (Y69), as well as their symmetry-related residues, are near the center of the active site pore and contribute substantially to the surface as shown in Figure 1. Residues near the center of symmetry interact with each other in pairs (Q67 and I68), while residues further away from the symmetry operator form individual binding surfaces (S65 and Y69). For example, two Q67 residues form hydrogen bonds with each other at the "floor" of the active site, while the other two symmetry-related Q67 residues form a similar hydrogen bonding pair at the "ceiling" of the pore. Q67 has been proposed to form extensive van der Waals interactions with the pteridine ring of folate in the R67 DHFR·folate crystal structure (*2*). (Density for only the pteridine ring of folate was observed, suggesting the *p*-aminobenzoic acid-Glu tail is disordered.) Two I68 residues also interact with each other on the "right-hand side" of the pore as well as a symmetry-related pair on the "left-hand side" of the pore. The backbone NH group of I68 is proposed to be involved in hydrogen bonding to the 4-oxo group of folate. In addition, the backbone NH of a symmetry-related I68 residue is proposed to interact indirectly with the N8 of folate through water molecule 124. A possible role for partial exclusion of solvent during catalysis may also be associated with I68. S65 and Y69 lie further from the 222 symmetry operator; thus, the binding surface contributed by each of the four symmetry-related residues is separate (i.e., they do not pair up with a symmetry-related S65 or Y69 residue on the active site pore surface to provide two contiguous surfaces as do Q67 and I68). A role for S65 and Y69 in binding folate has not yet been proposed; however, the hydroxyls from their side chains are pointing toward the pore and could be candidates for hydrogen bond formation.

Specific interactions between R67 DHFR and the cofactor have not been observed in a cocrystal structure; however, reduction of the pteridine ring by the nicotinamide ring of NADPH would require the NMN moiety (nicotinamide−ribose−P_i) to bind near the center of the pore. A model for bound NADPH was initially proposed by Narayana et al. (two folates and one NADPH; *2*); however, subsequent ITC binding studies indicated it must be incorrect as only two ligands bind (*6*). A more recent computational docking study using DOCK (docking based on van der Waals interactions; *7*, *8*) and SLIDE (docking based on H-bond formation; *9*−*11*) predicts roles for all four residues in binding NMN (E. E. Howell et al., submitted for publication). Briefly, the hydroxyl group of S65 may form a hydrogen bond (through an intermediary water molecule) to one of the ribose OHs (O2′) as well as to one of the oxygens of the P_i (O2) in NMN. Q67 may form a H-bond to one of the ribose OHs (O2′) through its NE2 group as well as form van der Waals interactions with several atoms of the nicotinamide ring through its side chain. I68 may form a pair of H-bonds between its backbone NH and O groups with the O and NH_2 of the carboxamide moiety of the nicotinamide ring, respectively. Several van der Waals interactions are also predicted between I68 and the ribose and P_i groups. The OH of Y69 may form a H-bond (through an intermediary water) to an oxygen off the P_i group. Y69 may also form several van der

Waals interactions through its CD1 and CE1 atoms with the ribose OHs.

Howell et al. (manuscript submitted for publication) propose numerous residues in R67 DHFR play a dual role in binding. For example, Q67 from both the B and D subunits has several contacts with the pteridine ring of substrate, while Q67 from the A and C subunits has several predicted contacts with the nicotinamide ring of the cofactor (see Figure 1). Other residues proposed to be involved in binding both ligands are I68 and Y69. This plasticity in binding is proposed to form a hot spot binding surface and allows an unusual mechanism for ligand binding and catalysis. Hot spots for protein−protein interactions have been noted and evaluated by mutagenesis and statistical analysis (*12*−*14*). A general trend proposed is the presence of residues that are amphipathic.

To evaluate the role of S65, Q67, I68, and Y69 residues in binding specificity as well as catalysis, mutant R67 DHFR genes were constructed and the effects of the mutations assessed.

MATERIALS AND METHODS

Construction and Expression of Mutant R67 DHFRs. A synthetic R67 gene, carried in pUC8, has been previously described (*15*). Site-directed mutagenesis using the appropriate primers was employed to construct S65A, Q67Y, Q67C, I68M, I68Q, I68L, Y69F, and Y69H mutations in the R67 DHFR gene by the PCR-based protocol outlined in the Quickchange kit from Stratagene. The PCR-based reactions, used in site-directed mutagenesis, required two complementary oligonucleotide primers containing the desired mutation. The coding strand sequences for each nucleotide primer are as follows: S65A, 5′-GGCTCACCCGGGC**(GCA)**GTACAGATCTATCC-3′; Q67Y, 5′-CCGGGCTCAGTA**(TAT)**ATCTATCCTGTTGCGGC-3′; Q67C, 5′-CCGGGCTCAGTA**(TGC)**ATCTATCCTGTTGCGGC-3′; I68L, 5′-GGGCTCAGTACAG**(TTG)**TATCCTGTTGCGGCG-3′; I68M, 5′-GGGCTCAGTACAG**(ATG)**TATCCTGTTGCGGCG-3′; I68Q, 5′-CCCGGGCTCAGTACAG**(CAG)**TATCCTGTTGCGGCG-3′; Y69F, 5′-GGGCTCAGTACAGATC**(TTC)**CCTGTTGCGGCG-3′; and Y69H, 5′-GGGCTCAGTACAAATC**(CAT)**CCTGTTGCGGCG-3′.

Concurrent removal of a *Bgl*II site allowed utilization of *Bgl*II restriction digests to screen for candidate mutant genes (except for the S65A mutant). To verify the presence of the mutation and to determine that no extraneous mutations occurred in the R67 DHFR gene, the DNA was sequenced using an ABI PRISM Dye Terminator Cycle Sequencing Ready Reaction kit from Perkin-Elmer (University of Tennessee Sequencing Facility, Knoxville, TN).

Escherichia coli cells (strain SK383) containing the mutant genes were grown in a modified version of TB medium (*16*). Cells were grown to late stationary phase in the presence of 200 μg/mL ampicillin and 20 μg/mL TMP. Cells were lysed using an alkaline lysis method (except for the Q67C variant), and Sephadex G-75, DEAE-Fractogel, and DEAE-Sephacyl chromatography steps were used in protein purification as previously described (*15*). In a final purification step, either a Mono-Q or a HiQ anion exchange column was used on a Pharmacia FPLC system. Sonication was used to lyse *E. coli* cells containing the Q67C mutant gene. Each protein was purified to homogeneity as determined by SDS−PAGE.

Steady State Kinetics. Steady state kinetic data were obtained using a Perkin-Elmer λ3a spectrophotometer interfaced with an IBM PS2 computer according to Howell et al. (*17*). The computer program UVSL3 (Softways, Moreno Valley, CA) was used to collect and analyze data. Assays were performed at 30 °C in a polybuffer containing 50 mM MES, 100 mM Tris, and 50 mM acetic acid at pH 7 (MTA buffer) (*18*). This polybuffer maintains a constant ionic strength from pH 4.5 to 9.5. Assays were performed by the addition of substrate (DHF) and cofactor (NADPH) followed by the addition of enzyme to initiate the reaction. To obtain k_{cat} and K_m values for each mutant, the concentration of NADPH was held constant at a subsaturating level while the concentration of DHF was varied. This process was repeated using four additional subsaturating concentrations of NADPH. The data were analyzed as described by Cleland (*19*).

Protein and ligand concentrations were determined spectrophotometrically. For all mutants, extinction coefficients were determined using the biuret assay (*20*). Ligand concentrations were determined using the following extinction coefficients: 28 000 M^{-1} cm^{-1} at 282 nm for DHF (*21*) and 6220 M^{-1} cm^{-1} at 340 nm for NADPH (*22*). The molar extinction coefficient used to assess DHFR reduction of DHF was 12 300 M^{-1} cm^{-1} (*23*).

Isothermal Titration Calorimetry. Binding affinities and the enthalpy associated with binding were monitored using isothermal titration calorimetry (ITC) as previously described (*6*, *24*). Briefly, measurements were carried out on a Microcal Omega ultrasensitive isothermal titration calorimeter equipped with a nanovoltmeter for improved sensitivity and connected to a circulating water bath for temperature control. The data were automatically collected by an IBM personal computer running DSCITC data acquisition software and were analyzed using Origin software provided by the manufacturer. The design and operation of this instrument have been described by Wiseman et al. (*25*). Samples typically consisted of ∼90−100 μM tetramer in MTA buffer (pH 8). Measurements were performed at 28 °C. Addition of ligand to buffer only was performed to allow baseline corrections. Data were fit to an interacting sites model where the stoichiometry of ligand binding was set equal to 2.

Gel Filtration Studies. Gel filtration studies, at pH 5 and 8, were carried out at 4 °C on a Pharmacia FPLC system using a Superose 12 (HR 10-30) column with a flow rate of 1.0 mL/min. The column was equilibrated in MTA buffer. Standard curves at pH 5 and 8 were produced by plotting the log molecular mass of protein standards (Pharmacia calibration kit) versus K_{av}. This allowed determination of the molecular mass and thus the oligomeric state of each R67 DHFR mutant. The K_{av} is defined as

$$K_{av} = (V_E - V_V)/(V_B - V_V) \quad (1)$$

where V_E is the elution volume, V_V is the void volume, and V_B is the bed volume of the column matrix.

pH Titration of Tryptophan Fluorescence. To monitor a pH-dependent equilibrium between tetramer and two

Table 1: Comparison of Steady State Kinetic Values for R67 DHFR Variants at pH 7.0

DHFR species (pH 7)	k_{cat} (s^{-1})	$K_{m(DHF)}$ (μM)	$K_{m(NADPH)}$ (μM)	$K_{m(DHF)mutant}/K_{m(DHF)wt}$	$K_{m(NADPH)mutant}/K_{m(NADPH)wt}$
wt R67 DHFR[a]	1.3 ± 0.07	5.8 ± 0.02	3.0 ± 0.06	–	–
S65A R67 DHFR	1.1 ± 0.10	4.0 ± 0.51	2.9 ± 0.57	0.69	0.97
Q67H R67 DHFR (pH 8)[b]	0.022 ± 0.003	0.16 ± 0.01	0.028 ± 0.001	0.027	0.009
Q67C R67 DHFR	0.10 ± 0.016	55 ± 10	26 ± 4.0	9.5	8.7
I68L R67 DHFR	0.32 ± 0.06	24 ± 3.0	26 ± 4.0	4.2	8.7
I68M R67 DHFR	0.17 ± 0.03	25 ± 3.0	21 ± 3.0	4.3	7.0
Y69F R67 DHFR	2.5 ± 0.04	44 ± 2.1	66 ± 2.6	7.6	22
Y69H R67 DHFR	0.014 ± 0.002	46 ± 4.5	176 ± 6.0	7.9	59

[a] Values from ref *15*. [b] Values from ref *24*.

protonated dimers in wild-type or mutant R67 DHFRs, given by the following equation

$$T + 2nH^+ \overset{K_{overall}}{\rightleftharpoons} 2DH_n \quad (2)$$

tryptophan fluorescence was monitored as a function of pH on a Perkin-Elmer LS-5B luminescence spectrometer (*26*). The emission spectra for the DHFRs (excitation at 295 nm) were measured from 300 to 450 nm at each pH during the titrations. The intensity-averaged emission wavelength, $\langle\lambda\rangle$, for each emission spectrum was calculated using the equation

$$\langle\lambda\rangle = \sum(I_i\lambda_i)/\sum(I_i) \quad (3)$$

where I is the intensity and λ is the wavelength (*27*). $\langle\lambda\rangle$ is an integral measurement that is less sensitive to noise. Data were fit to the following equation describing the linkage between the tetramer and protonated dimer equilibrium (*26*):

$$Flu_{obs} = \{(Flu_{di} - Flu_{tet})[[H]^{2n}/(4K_{overall}P_{tot})][-1 + (1 + 8K_{overall}P_{tot}/[H]^{2n})^{1/2}]\} + Flu_{di} \quad (4)$$

where $K_{overall} = ([tetramer][H]^{2n})/([dimer]H_{2n}^2)$ in units of M, M^2, or M^3 for $n = 1$, 1.5, or 2, respectively; Flu_{obs} is the observed fluorescence; Flu_{di} and Flu_{tet} are the calculated limits for dimer and tetramer fluorescence at low and high pH, respectively; and P_{tot} is the total protein concentration in terms of dimer (*26*). The program SAS (statistical analysis software) was employed to fit the data using nonlinear regression. To facilitate comparison, the data were normalized by fitting to the equation $F_{app} = (Y_{obs} - Y_{pH\ 8})/(Y_{pH\ 5} - Y_{pH\ 8})$, where F_{app} is a fractional value between 0 and 1 and Y_{obs}, $Y_{pH\ 8}$, and $Y_{pH\ 5}$ are the optical values associated with the observed pH and the pH limits of 8 and 5, respectively.

Circular Dichroism. Circular dichroism spectra of mutant and wt R67 DHFRs in 10 mM KH_2PO_4 at pH 5.0 and 8.0 were obtained at 22 °C using an Aviv 202 circular dichroism spectrometer. The cell path length was 1 cm. Ten spectra were acquired per sample using 1 nm steps and 2 s integrations, and an averaged spectrum was calculated. An essentially flat buffer baseline scan was then subtracted from the average protein scan. The CD data are described as mean residue ellipticity by taking 108 Da as the mean residue molecular mass.

RESULTS

The S65A, Q67Y, Q67C, I68M, I68Q, I68L, Y69F, and Y69H mutant genes were constructed and sequenced as described above. To evaluate which mutations were most functional, *E. coli* cells were transformed with plasmid DNA containing the mutant genes and screened for the ability to confer resistance to trimethoprim. All mutant genes except the Q67Y construct provided resistance to the antibiotic at 20 μg/mL. Only the Q67H, I68Q, and Y69H mutant genes could not confer TMP resistance at TMP concentrations of ≥ 50 μg/mL.

The correct molecular masses for the Q67C, I68L, I68M, and Y69F mutants were confirmed by electrospray ionization mass spectrometry (ESI-MS) on a Thermo Finnigan LCQ-DECA ion trap. The correct mutation site was confirmed for each of these mutants by digestion with the endoproteinase GluC. The resultant peptide mixtures were desalted with a C18 ZipTip and directly infused into the ion trap mass spectrometer. The peptide containing the suspected mutation site was isolated, and MS/MS was performed to obtain sequence information. To ensure the Q67C mutant did not form a disulfide bond with a symmetry-related cysteine residue, an exact mass of the intact protein was obtained by ESI-MS on an Ion Spec Fourier transform-ion cyclotron resonance mass spectrometer. These data and a novel technique for detecting mutation sites in the intact protein are described in detail in a separate report (manuscript in preparation). The Q67C mutant had a measured mass of 8405.15 Da (monomer), consistent with all the cysteines being reduced.

Steady State Kinetic Analysis. Steady state kinetic data are given in Table 1 for mutant and wt R67 DHFRs. All kinetic data were obtained at pH 7 with the exception of the data for Q67H R67 DHFR. This mutant was constructed and characterized at pH 8 as previously described (*24*). The kinetic values for the S65A mutant are comparable to those of wt R67 DHFR. In contrast, the Q67H mutation tightens binding to DHF and NADPH by 36- and 110-fold, respectively. This is the only mutation that tightens binding. The Q67C mutation weakens binding to both DHF and NADPH by approximately 9-fold. The I68L and I68M mutations have similar effects, weakening binding to DHF and NADPH by approximately 4- and 7−9-fold, respectively. The Y69F mutation weakens binding to DHF and NADPH by 8- and 20-fold, respectively, while the Y69H mutation weakens binding to DHF and NADPH by approximately 8- and 60-fold, respectively.

The changes in *both* NADPH and DHF K_m values suggest the Q67, I68, and Y69 residues play a dual role and contribute to binding of both ligands. Furthermore, since the $[K_{m(DHF)mutant}]/[K_{m(DHF)wt}]$ ratio and the $[K_{m(NADPH)mutant}]/[K_{m(NADPH)wt}]$ ratio are mostly similar, these residues display very little specificity for DHF versus NADPH binding. For example, in the context of 36−110-fold tighter binding of ligands in the Q67H R67 DHFR, there is only a 3-fold

preference for NADPH binding. Also for the Y69F R67 DHFR, in the context of 7.6−22-fold weaker binding, there is only a 3-fold preference for DHF binding. The largest preference observed is a 7.5-fold preference for substrate binding over NADPH, which occurs in the Y69H mutant.

Effects on k_{cat} are variable and depend on the residue and the particular substitution. No significant effects are observed for the S65A mutant, while for the Q67 mutants, a loss in activity is observed. Since substantial substrate and cofactor inhibition is observed for the Q67H mutant, its k_{cat} value is given at pH 8 and is derived by global fitting of kinetic data by FITSIM (*24*). For wt DHFR, k_{cat} at pH 8 is 8.8 min^{-1}, indicating a 6.8-fold decrease in activity is associated with the Q67H mutation. For the Q67C mutant, a 13-fold decrease in k_{cat} is observed when compared to that of wt R67 DHFR at pH 7. A Q67Y mutant was also constructed; however, protein production levels were low, and the gene did not confer TMP resistance upon host *E. coli*, implying diminished catalytic efficiency. For the I68 mutants, the I68M substitution has a slightly larger effect on k_{cat} with an 8-fold decrease, while the I68L mutant exhibits an only 4.2-fold decrease. An I68Q mutant was constructed; however, the ability of the gene to confer TMP resistance was minimal, and an initial protein purification gave low yields with marginal activity, suggesting less conservative substitutions decrease catalytic activity more dramatically. For Y69 substitutions, the Y69F mutant was conservative and resulted in a 2-fold enhancement of k_{cat}. However, the Y69H mutation decreased k_{cat} approximately 90-fold. These results indicate the binding surface contributed by residues 67−69 is involved in stabilization of the transition state.

A low level of substrate inhibition was observed for the I68L mutant, and a more noticeable level was associated with the I68M mutant. These observations indicate that the ternary complex may be slightly different in these mutants and/or the degree of cooperativity between ligands may have changed.

ITC. To determine the effect of selected mutations on ligand binding and cooperativity, isothermal titration calorimetry was employed to monitor NADPH binding. Best fits of wt R67 DHFR data indicate it binds two NADPH molecules, with negative cooperativity (*6*). Figure 2 shows a representative ITC titration between I68L R67 DHFR and NADPH. Best fits of the data for all the mutants, which yield K_d values as well as the ΔH associated with binding of NADPH, are given in Table 2. All the mutants display negative cooperativity between two bound NADPH molecules. Except for Q67H R67 DHFR, all mutants display weaker affinity for NADPH in comparison to the wt values. Finally, the difference in affinity between the two bound NADPH molecules remains relatively the same (from a 38-fold difference between wt sites to a 23-fold difference between Q67H and I68L sites). This latter observation indicates the cooperativity between two bound NADPH molecules is not affected much by the mutations.

Gel Filtration. To eliminate the possibility that the changes in catalytic efficiency described above might be due to alterations in the oligomeric state of the mutant R67 DHFRs, their elution patterns at pH 5 and 8 were analyzed using molecular sieving chromatography. Values corresponding to the estimated molecular mass of mutant and wt R67 DHFRs are shown in Table 3. At pH 5.0, wt R67 DHFR elutes from an FPLC Superose 12 column as a dimer, and at pH 8.0, it elutes as a tetramer. The mutant proteins have estimated molecular masses similar to those of wt R67 DHFR at pH 5.0 and 8.0. The amino acid sequence predicts molecular masses of 16 860 and 33 720 Da for dimeric and tetrameric R67 DHFR, respectively (*26*). Abberant molecular mass

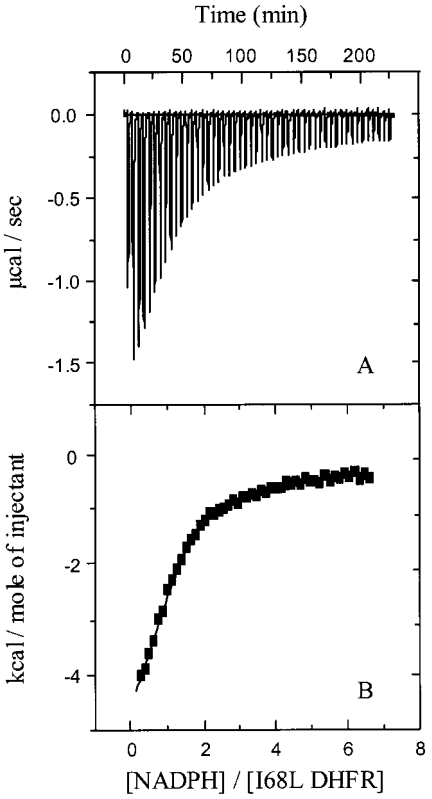

FIGURE 2: ITC titration involving NADPH binding to I68L R67 DHFR. Panel A shows the series of peaks generated from the heat liberated upon NADPH binding. As the protein approaches saturation, less of each subsequent addition is bound, so the peaks decrease in height. The protein concentration was 87 μM tetramer. Panel B shows the heat liberated per mole of titrant added vs the cofactor/protein tetramer molar ratio. The smooth line shows the fit to the data for a model which describes ligand binding to two interacting sites exhibiting negative cooperativity. Average values for K_d and ΔH are given in Table 2. Note the heat associated with the first peak in panel A was not included in panel B or in the data analysis.

Table 2: Comparison of K_d Values Describing Binding of NADPH to R67 DHFR Variants at pH 8.0 Monitored by ITC[a]

DHFR species	K_d (μM)	K_{d2}/K_{d1}	ΔH (kcal/mol)	no. of experiments
wt R67 DHFR[b]	2.5 ± 0.15	38	−8.6 ± 0.02	2
	95 ± 4		−5.8 ± 2.5	
S65A R67 DHFR	3.0 ± 0.05	30	−9.1 ± 0.06	2
	89 ± 1.6		−7.9 ± 0.42	
Q67H R67 DHFR[c]	0.027 ± 0.008	23	−4.8 ± 0.10	2
	0.62 ± 0.11		−2.5 ± 0.40	
I68L R67 DHFR	23 ± 2.1	23	−5.6 ± 0.12	2
	520 ± 54		−4.6 ± 0.35	
Y69F R67 DHFR	16 ± 1.1	31	−2.6 ± 0.05	2
	490 ± 36		−4.7 ± 0.09	

[a] The ITC fit reports microscopic constants (k_1 and k_2); however, the K_d values below are the macroscopic constants (K_1 and K_2). The statistical relationship between microscopic and macroscopic constants is $K_{d1} = {}^1/_2 k_{d1}$ and $K_{d2} = 2k_{d2}$ (*28*). Values reported for all mutants are fit to an interacting sites model which sets the ligand stoichiometry at 2.0. [b] From ref *6*. [c] From ref *24*.

Table 3: Calculated Molecular Masses for R67 DHFRs As Determined by Molecular Sieving Chromatography

DHFR species	MW (Da) pH 8.0	MW (Da) pH 5.0
wt R67 DHFR	40000 ± 990	26000 ± 920
S65A R67 DHFR	40000 ± 600	26000 ± 300
Q67C R67 DHFR	41000 ± 110	29000 ± 230
I68L R67 DHFR	43000 ± 980	29000 ± 930
I68M R67 DHFR	42000 ± 160	27000 ± 950
Y69F R67 DHFR	43000 ± 990	26000 ± 920
Y69H R67 DHFR	40000 ± 760	28000 ± 620

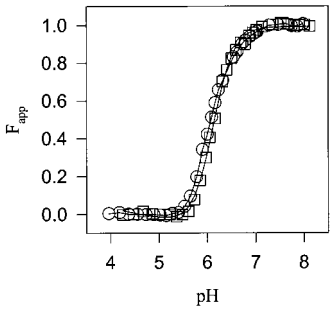

FIGURE 3: pH titration of R67 DHFRs monitored by fluorescence. The intensity-averaged wavelength, $\langle\lambda\rangle$, for wt and Y69F R67 DHFRs (○ and □, respectively) was monitored as a function of pH. The protein concentration of wt and Y69F R67 DHFRs was 2 μM. The data were each fit to eq 4, and best fit values are listed in Table 4. For ease of comparison, data were converted to F_{app}.

Table 4: Best Fit Values for the pH-Dependent Dissociation of Tetramer into Two Dimers As Monitored by Fluorescence

DHFR species	$K_{overall}$ ($=K_a^{2n}/K_d$) for $n = 3$ in units of M^2
wt R67 DHFR	$1.2 \times 10^{-13} \pm 4.00 \times 10^{-14}$
S65A R67 DHFR	$2.21 \times 10^{-13} \pm 4.14 \times 10^{-14}$
I68L R67 DHFR	$5.73 \times 10^{-14} \pm 1.62 \times 10^{-14}$
I68M R67 DHFR	$1.04 \times 10^{-13} \pm 7.12 \times 10^{-14}$
Y69F R67 DHFR	$4.79 \times 10^{-13} \pm 1.13 \times 10^{-13}$
Y69H R67 DHFR	$2.02 \times 10^{-13} \pm 8.12 \times 10^{-14}$

estimates determined by gel filtration are not unusual as the hydrodynamic volume or shape of the molecule as well as the size affects elution (*29*).

pH Titration of Tryptophan Fluorescence. To examine any subtle effects the mutations might have had on the tetramer to two dimers equilibrium, steady state tryptophan fluorescence was monitored as a function of pH. Symmetry-related H62, H162, H262, and H362 residues located at the dimer interfaces are involved in stabilizing tetrameric R67 DHFR. Titration of these residues results in tetramer destabilization and protonated dimer formation. Since W38 also occurs at the dimer−dimer interfaces, tryptophan fluorescence can be used to monitor whether the W38 environment is solvent-exposed (dimer) or buried in a hydrophobic environment (tetramer).

The pH titration data for mutant and wt R67 DHFRs are listed in Table 4. The $K_{overall}$ values for each mutant are similar to those for wt R67 DHFR with the best fit occurring when $n = 3$, where n corresponds to the number of protons added to the dimer−dimer interfaces resulting in dissociation. To aid comparison, the data were converted to F_{app} values, and the profiles for the wt and Y69F mutant DHFRs are shown in Figure 3. Minimal changes might be expected for the I68 and Y69 mutants as they are not near the dimer−dimer interface. Q67 is, however, at the bottom of the dimer−dimer interface, and mutation of this residue could alter the stability of the tetramer. The F_{app} plot for Q67H shows that the mutation slightly destabilizes the tetramer (*24*). Alteration (or removal) of the Q67−Q367 interactions by the Q67H mutation may be the mechanism of destabilization. In this study, the data for the Q67C mutant visually appeared to display a titration (data not shown); however, since the overall signal change was small and pre- and post-transition slopes were present, the fitting program could not obtain a fit with reasonable errors. Thus, quantitation of the $K_{overall}$ for the Q67C mutant was not obtained. For the other mutants, the F_{app} plots clearly show that the mutations minimally perturb the tetramer to two dimers equilibrium.

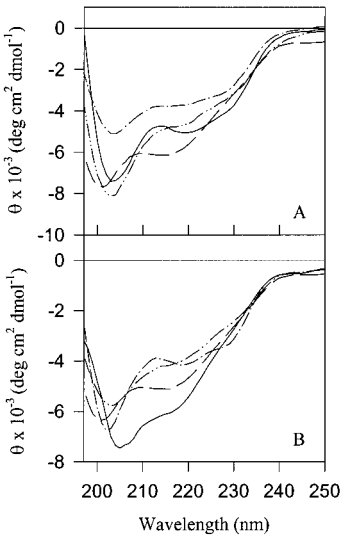

FIGURE 4: Assessment of secondary structure in R67 DHFRs by CD. Panel A displays the scans of various representative DHFRs at pH 8 where the proteins are tetrameric: wt R67 DHFR (—), Q67C R67 DHFR (—••—), I68L (— — —), and Y69H R67 DHFR (—•—). Panel B displays the scans at pH 5 where the proteins are dimers: wt R67 DHFR (—), Q67C R67 DHFR (—••—), I68L (— — —), and Y69H R67 DHFR (—•—). Data are presented as the mean residue ellipticity, θ, by taking 108 Da as the mean residue molecular mass.

Circular Dichroism. To evaluate the effect of the mutations in the active site pore on the overall secondary and tertiary structure of R67 DHFR, CD spectra were obtained at pH 5.0 and 8.0 and are depicted in Figure 4. For most cases, smaller signals are observed for the mutants than for wt, particularly at pH 5. The CD data are consistent with the protein being folded and alteration of the conformation (i.e., oligomerization state) as a function of pH. The differences in the CD signal may reflect subtle changes in the structure and/or different contributions of aromatic groups to the signal due to altered local environments associated with the mutations (*30*).

DISCUSSION

The S65, Q67, I68, and Y69 Residues Comprise 47% of the Binding Surface. Single mutations in the R67 DHFR gene result in four mutations per homotetramer. Since R67 DHFR possesses a single active site pore, the effect of four concurrent mutations on the ligand binding surface can be profound. For example, the cumulative effect of four mutations at either K32, W38, or H62 at the dimer−dimer

interfaces results in destabilization of the tetramer such that only dimers are formed (*31*−*33*). For the mutations in the study presented here, the S65 residues contribute 5% of the binding surface, Q67 residues 14%, I68 residues 19%, and Y69 residues 9%. The total surface area (Connolly) contributed by the S65, Q67, I68, and Y69 residues is 47% of the total available (generated from residues 32, 36, 46, and 64−69). Thus, large effects on ligand binding may be expected for mutations at these residues.

A corollary of four mutations occurring simultaneously per active site pore is that mutations most likely need to be conservative to not have very profound effects on protein structure and/or function. For example, the Y69F mutant is quite active, while the Y69H mutant is not. In a second example, the I68L and I68M mutants have similar steady state kinetic values, and both are less efficient than wt R67 DHFR. However, the I68Q mutant gene only conferred resistance to a low level of TMP, and from an initial purification of the I68Q mutant protein, it was clear that its activity level was quite low (data not shown).

How Can the Effect of the Mutations Be Understood? In *E. coli* chromosomal DHFR, mutations in the DHF binding pocket affect DHF K_d values by 1700−0.5-fold, while K_d values for NADPH are concurrently altered 3.33−0.45-fold (*34* and references therein). The general trend observed in these mutants is that DHF, but not NADPH binding, is affected. A similar trend is observed for mutations in the NADPH binding pocket with up to 23-fold increases for NADPH K_d values, while DHF K_d values are altered by up to only 4-fold. These results indicate the effects of the mutations are mostly local, and focus on the ligand whose contacts are disrupted. Lesser to no effects are observed on binding of the second ligand.

In contrast to the above effects of mutations in chromosomal DHFR, R67 DHFR shows a different pattern. The D_2 symmetry in R67 DHFR dictates that the effect of a mutation on a binding site must be paralleled by a similar effect at the symmetry-related sites. This is most clearly seen in the ITC data which monitor binding of two NADPH molecules. From an examination of the binding data in Table 2, the mutations at Q67, I68, and Y69 clearly alter both NADPH binding events. For the Q67H mutant, both NADPH molecules are bound approximately 100 times more *tightly*.[3] In contrast, for the I68L mutant, both NADPH molecules are bound approximately 10 times more *weakly*. While the effects of the various mutations on the K_d values range over 3 orders of magnitude, the difference in affinity between the bound NADPH pairs is barely altered. A ratio of K_{d2} (for the second NADPH) to K_{d1} (for the first NADPH) ranges from a 23-fold (Q67H and I68L) to a 38-fold difference (wt). An effect on the K_{d2}/K_{d1} ratio that is this small suggests the mutations influence the affinity for NADPH at both symmetry-related sites to an equal extent.

The ratio of K_{d2} to K_{d1} for pairs of bound NADPH molecules may also be considered a measure of the cooperativity between bound NADPH molecules. This alternative, linked point of view states that when binding of one ligand is altered, binding of the second ligand may also be changed depending on the extent of interaction between ligands. Thus, these studies also address the relationship between ligand cooperativity and symmetry effects in R67 DHFR.

The effects of symmetry and interligand cooperativity can be unrelated if the binding sites are separate. For this simple situation, a mutation should alter both K_d values equally. However, if the ligands interact when bound, then symmetry effects and ligand cooperativity are expected to show some degree of linkage. This is especially true if the ligands bind near the center of the active site pore near the 222 symmetry operator. For the case of negatively interacting sites, typified by NADPH binding, the first NADPH is proposed to bind and cross the center of symmetry in R67 DHFR (*6*). This results in loss of a symmetry-related site and a weakened affinity for the second NADPH molecule. The effects of mutations on this model rely on steric hindrance, so if the position of the NADPH bound first is not drastically altered by the mutation, minimal effects on NADPH cooperativity may be expected. If the position of the NADPH bound first is greatly altered, the position of the NADPH bound second could also be altered, and this difference reflected by a larger change in K_d. That the cooperativity between bound NADPH molecules changes minimally in our series of mutants suggests the relative position of the bound NADPH pairs must not be too drastically altered with respect to each other.

The extent of linkage between symmetry and cooperativity between NADPH and DHF can be broached by considering the steady state kinetic data. When binding is assessed using the kinetic data in Table 1, the Q67, I68, and Y69 mutations can be seen to alter K_m values for both NADPH and DHF. The Y69F mutant displays 8-fold *weaker* binding to DHF and 22-fold *weaker* binding to NADPH than wt. In contrast, when compared to wt values, the Q67H mutant displays 36- and 110-fold *tighter* binding to DHF and NADPH, respectively. In the context of these changes in K_m, which vary by up to 3 orders of magnitude, the ability of the mutations to preferentially alter NADPH versus DHF binding appears to be marginal. For example, the Q67H mutant *enhances* NADPH binding (compared to DHF) by only 3-fold, while the Y69F mutant *weakens* NADPH binding (compared to DHF) by 3-fold. The I68L and I68M mutants all have an approximately 2-fold preference for DHF binding, while the Y69H mutant has a 7-fold preference for DHF binding. Again, while changes are observed, the differential effects they have on binding one ligand versus the other are orders of magnitude lower. However, in contrast to the ITC data, which essentially showed no change in the cooperativity between two bound NADPH molecules, the kinetic data hint at some minimal alterations in cooperativity between NADPH and DHF.

The issue of whether the mutations exert their effect by affecting both the NADPH and DHF binding sites or by affecting the cooperativity between ligands may be a moot point if cooperativity is an important component in catalysis for this enzyme. Consider a multipoint attachment model to describe ligand binding (*38*). In this model, at least three points are required to bind the ligand with sufficient uniqueness for a reaction to display stereospecificity. A two-point attachment would allow rotation and result in racemic product mixtures. If numerous attachment points in R67 DHFR involve NADPH·DHF interactions, then cooperativity is an essential part of the mechanism. The resulting transition

[3] Tighter binding for the Q67H mutant may arise from stacking interactions between the imidazole ring and the folate pteridine ring (or the NADPH nicotinamide ring) (*35*−*37*).

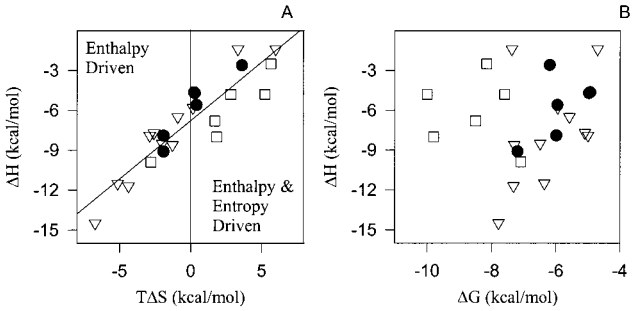

FIGURE 5: Thermodynamic analysis of binding. Panel A shows a plot of $T\Delta S$ vs ΔH for various mutant R67 DHFRs and various ligands. Values for NADPH binding to the mutants described in this study are given by ●. Values for binding of various ligands to wt R67 DHFR were taken from ref *6*, while values for binding of various ligands to Q67H R67 DHFR were taken from ref *24*. Twenty-three different data points are given. The slope of the line is 0.90, and the correlation coefficient is 0.82. Panel B shows a plot of ΔH vs ΔG where there is no correlation.

state in R67 DHFR requires some degree of interaction between the pteridine ring of DHF and the nicotinamide ring of NADPH. This view would be more consistent with an *endo* conformer of the transition state (where the nicotinamide ring overlaps the more bulky side of the pteridine ring) than with an *exo* conformer (with minimal overlap of the pteridine and nicotinamide rings; *39*, *40*). The *endo* transition state for DHFR has been shown to be 2−8 kcal/mol more stable than the *exo* transition state due to the inter-ring interactions (*41*). The *exo* model describes the transition state associated with chromosomal *E. coli* DHFR as this active site constellation constrains how ligands bind and funnels the transition state toward the *exo* conformer. In contrast to those for chromosomal DHFR, the results obtained in these mutagenesis studies are consistent with an *endo* model for the transition state in R67 DHFR. Interligand NOE NMR data also favor this model (*42*) as do docking studies focused on generating a ternary complex model by Howell et al. (manuscript submitted for publication).

How Unique Are the NADPH and DHF Binding Sites? Using computer docking algorithms, a model of the R67 DHFR·NMN·Fol1 ternary complex has been proposed (E. E. Howell et al., manuscript submitted for publication). Using a symmetry operation to overlap the two proposed binding sites indicates that the nicotinamide ring of NADPH occupies a position very similar to that of the N5- and N8-containing ring of the pteridine ring of folate. This partial overlap of sites also predicts that the mutations will have effects on binding both DHF and NADPH.

Enthalpy−Entropy Compensation? Binding of NADPH produces exothermic ITC isotherms for all the mutants. From the K_d values given in Table 2, values for ΔG can be calculated using the relationship $\Delta G = -RT \ln K_a$, where K_a is the association constant and equals $1/K_d$. From this, $T\Delta S$ can be calculated from the relationship $\Delta G = \Delta H - T\Delta S$. A plot of ΔH versus $T\Delta S$ is reasonably linear as shown in Figure 5, while a plot of ΔH versus ΔG shows no trends (Figure 5B). Additional data points describing binding of DHF, folate, CB3717 (a folate analogue), and $NADP^+$ in various binary and ternary complexes are also shown for wt and Q67H R67 DHFRs (data taken from refs *6* and *24*). These additional points strengthen the linear correlation between ΔH and $T\Delta S$ as well as extend the observable range.

Alteration of the ligand or the enzyme can be expected to result in different degrees of hydrogen bonding and van der Waals contacts which in turn can alter the degrees of freedom of the ligand and amino acid side chain (*43*, *44*). The former would affect ΔH and the latter $T\Delta S$. Solvent reorganization may be involved in the effects of different ligands and mutant enzymes on ΔH and $T\Delta S$ (*45*, *46*). Finally, any proton exchange between enzyme and buffer to which ligand binding may be coupled could also be perturbed by use of a different ligand or a different mutant and result in a concomitant change in the thermodynamics of ligand binding. With these caveats in mind, one observation from Figure 5 is that most of the wt interactions (▽) are enthalpically driven, while most of the mutant interactions (● and □) possess both enthalpic and entropic contributions. In addition, the most negative ΔH values arise during binding of two ligands per active site pore in the wt enzyme (R67 DHFR·DHF·$NADP^+$, R67 DHFR·2folate, and R67 DHFR·2CB3717), providing some support to the notion that ligand−ligand interactions may be important to binding and, ultimately, catalysis.

What Are the Roles of the S65, Q67, I68, and Y69 Residues? From the steady state kinetic analyses, it is clear that the Q67, I68, and Y69 mutations affect both K_m and k_{cat} values. The S65 mutant did not alter kinetic or ITC values significantly, indicating it does not interact directly with ligands. Alternatively, from the docking results using SLIDE, S65 may interact indirectly with ligands through an intermediary water molecule, and perhaps the S65A substitution is not sufficient to perturb the water structure.

There are several patterns observed for mutations at Q67, I68, or Y69. The most benign mutation is Y69F, as the k_{cat} is slightly enhanced while the k_{cat}/K_m is decreased. This result indicates that Y69F destabilizes both the ground and transition states, although the former more than the latter (*38*). This behavior minimally corresponds to a "uniform binding effect" and may indicate a slight "enhancement of an elementary step" (*47*). All the other mutations (except Q67H) show decreased k_{cat} values and even greater decreases in k_{cat}/K_m values. These results indicate destabilization of the ES complex and even greater destabilization of the transition state. This would correspond to a "differential binding effect" (*47*). The last mutational pattern occurs with the Q67H mutant. Tighter binding to NADPH and DHF is observed as well as a decreased k_{cat} value (*24*). While tighter binding of NADPH and DHF in the Q67H mutant may imply ligand binding in wt R67 DHFR involves some degree of ground state destabilization, the concurrent tighter binding of ligand at the symmetry-related sites results in substantial cofactor and substrate inhibition.

Is R67 DHFR a Primitive Enzyme? Our results indicate R67 DHFR provides a very different active site constellation than chromosomal DHFR or most other enzymes. The 222 symmetry of the structure, combined with the single active site pore, generates an unusual approach to catalysis. One consequence of this symmetry is that the presence of four symmetry-related mutations can profoundly affect catalysis. Therefore, it is difficult for this enzyme to acquire mutations that facilitate catalysis and evolve to a high efficiency. Also linked to the symmetry is the proposal that interligand cooperativity may be quite important in binding. The ability of the ligands to interact may somewhat mitigate the necessity of the ligands to bind to unique sites in the enzyme.

Instead, the enzyme appears to possess a binding hot spot that can accommodate (with some degree of overlap) both folate and NADPH. Finally, the above data are consistent with the notion that R67 DHFR utilizes an *endo* conformer of the transition state, involving cooperativity between ligands during binding. All these observations suggest R67 DHFR is a good model for a primitive enzyme.

ACKNOWLEDGMENT

We thank the Organic and Biological Mass Spectrometry group at Oak Ridge National Laboratory for performing the mass spectrometry analyses.

REFERENCES

1. Matthews, D. A., Smith, S. L., Baccanari, D. P., Burchall, J. J., Oatley, S. J., and Kraut, J. (1986) *Biochemistry 25*, 4194−4204.
2. Narayana, N., Matthews, D. A., Howell, E. E., and Xuong, N. H. (1995) *Nat. Struct. Biol. 2*, 1018−1025.
3. Wlodawer, A., Miller, M., Jaskolshki, M., Sathyanarayana, B. K., Baldwin, E., Weber, I. T., Selk, L. M., Clawson, L., Schneider, J., and Kent, S. B. H. (1989) *Science 245*, 616−621.
4. Wojtczak, A., Neumann, P., and Cody, V. (2001) *Acta Crystallogr. D57*, 957−967.
5. Arnone, A. (1972) *Nature 247*, 146−147.
6. Bradrick, T. D., Beechem, J. M., and Howell, E. E. (1996) *Biochemistry 35*, 11414−11424.
7. Kuntz, I. D., Blaney, J. M., Oatley, S. J., Langridge, R., and Ferrin, T. E. (1982) *J. Mol. Biol. 161*, 269−288.
8. Shoichet, B. K., and Kuntz, I. D. (1993) *Protein Eng. 6*, 723−732.
9. Schnecke, V., and Kuhn, L. A. (1999) *Proc. Int. Conf. Intell. Syst. Mol. Biol.*, 242−251.
10. Schnecke, V., Swanson, C. A., Getzoff, E. D., Tainer, J. A., and Kuhn, L. A. (1998) *Proteins: Struct., Funct., Genet. 33*, 74−87.
11. Raymer, M. L., Sanschagrin, P. C., Punch, W. F., Venkataraman, S., Goodman, E. D., and Kuhn, L. A. (1997) *J. Mol. Biol. 265*, 445−464.
12. Delano, W. L., Ultsch, M. H., de Vos, A. M., and Wells, J. A. (2000) *Science 287*, 1279−1283.
13. Bogan, A. A., and Thorn, K. S. (1998) *J. Mol. Biol. 280*, 1−9.
14. Hu, Z., Ma, B., Wolfson, H., and Nussinov, R. (2000) *Proteins 39*, 331−342.
15. Reece, L. J., Nichols, R., Ogden, R. C., and Howell, E. E. (1991) *Biochemistry 30*, 10895−10904.
16. Tartof, K. D., and Hobbs, C. A. (1987) *Gibco-Bethesda Research Labs Focus 9*, 12.
17. Howell, E. E., Warren, M. S., Booth, C. L. J., Villafranca, J. E., and Kraut, J. (1987) *Biochemistry 26*, 8591−8598.
18. Ellis, K. J., and Morrison, J. F. (1982) *Methods Enzymol. 87*, 405−426.
19. Cleland, W. W. (1963*) Biochim. Biophys. Acta 67*, 104−137.
20. Gornall, A. G., Bardawill, C. J., and David, M. M. (1949) *J. Biol. Chem. 177*, 751−766.
21. Blakley, R. L. (1960) *Nature 188*, 231−232.
22. Horecker, B. L., and Kornberg, A. (1948) *J. Biol. Chem. 175*, 325−390.
23. Baccanari, D., Phillips, A., Smith, S., Sinski, D., and Burchall, J. (1975) *Biochemistry 14*, 5267−5273.
24. Park, H., Bradrick, T. D., and Howell, E. E. (1997) *Protein Eng. 10*, 1415−1424.
25. Wiseman, T., Williston, S., Brandts, J. F., and Lin, L.-N. (1989) *Anal. Biochem. 179*, 131−137.
26. Nichols, R., Weaver, C. D., Eisenstein, E., Blakley, R. L., Huang, T.-H., Huang, F.-Y., and Howell, E. E. (1993) *Biochemistry 32*, 1695−1706.
27. Royer, C. A., Mann, C. J., and Matthews, C. R. (1993) *Protein Sci. 2*, 1844−1852.
28. Cantor, C. R., and Schimmel, P. R. (1980) *Biophysical Chemistry Part II, The Behavior of Biological Macromolecules*, W. H. Freeman & Co., San Francisco.
29. Potschka, M. (1987) *Anal. Biochem. 162*, 47−64.
30. Woody, R. W. (1995) *Methods Enzymol. 246*, 34−71.
31. West, F. W., Seo, H.-S., Bradrick, T. D., and Howell, E. E. (2000) *Biochemistry 29*, 3678−3689.
32. Hamilton, B. (1977) Masters Thesis, University of Tennessee, Knoxville, TN.
33. Park, H., Zhuang, P., Nichols, R., and Howell, E. E. (1997) *J. Biol. Chem. 272*, 2252−2258.
34. Miller, G. P., and Benkovic, S. J. (1998) *Chem. Biol. 5*, R105−R113.
35. Brocchierei, L., and Karlin, S. (1994) *Proc. Natl. Acad. Sci. U.S.A. 91*, 9297−9301.
36. Hakoshima, T.-I., Itoh, T., Tomita, K.-I., Goda, K., Nishikawa, S., Morioka, H., Uesugi, S.-I., Ohtsuka, E., and Ihehara, M. (1992) *J. Mol. Biol. 223*, 1013−1028.
37. Sapse, A. M., Schweitzer, B. S., Diker, A. P., Bertino, J. R., and Frecer, V. (1992) *Int. J. Pept. Res. 39*, 18−23.
38. Fersht, A. R. (1999) *Structure and Mechanism in Protein Science: A Guide to Enzyme Catalysis and Protein Folding*, W. H. Freeman & Co., New York.
39. Andres, J., Moliner, V., Safont, V. S., Domingo, L. R., Picher, M. T., and Krechl, J. (1996) *Bioorg. Chem. 24*, 10−18.
40. March, J. (1992) *Advanced Organic Chemistry: Reactions, Mechanisms and Structure*, 4th ed., John Wiley and Sons, New York.
41. Castillo, R., Andres, J., and Moliner, V. (1999) *J. Am. Chem. Soc. 121*, 12140−12147.
42. Li, D., Levy, L. A., Gabel, S. A., Lebetkin, M. S., DeRose, E. F., Wall, M. J., Howell, E. E., and London, R. E. (2001) *Biochemistry 40*, 4242−4252.
43. Gilli, P., Ferretti, V., Gilli, G., and Borea, P. A. (1994) *J. Phys. Chem. 98*, 1515−1518.
44. Dunitz, J. D. (1995) *Chem. Biol. 2*, 709−712.
45. Chervenak, M. C., and Toone, E. J. (1994) *J. Am. Chem. Soc. 116*, 10533−10539.
46. Grunwald, E., and Steel, C. (1995) *J. Am. Chem. Soc. 117*, 5687−5692.
47. Albery, J. W., and Knowles, J. R. (1976) *Biochemistry 15*, 5631−5640.

BI0110544